Structure, Vol. 13, 1131–1141, August, 2005, ©2005 Elsevier Ltd All rights reserved. DOI 10.1016/j.str.2005.04.020

Allosteric Inhibition of Aminoglycoside Phosphotransferase by a Designed Ankyrin Repeat Protein

Andreas Kohl,[1,2] Patrick Amstutz,[1,2] Petra Parizek,[1,2] H. Kaspar Binz,[1] Christophe Briand,[1] Guido Capitani,[1] Patrik Forrer,[1] Andreas Plückthun,[1,*] and Markus G. Grütter[1,*]

[1]Department of Biochemistry
University of Zürich
Winterthurerstrasse 190
CH-8057 Zürich
Switzerland

Summary

Aminoglycoside phosphotransferase (3′)-IIIa (APH) is a bacterial kinase that confers antibiotic resistance to many pathogenic bacteria and shares structural homology with eukaryotic protein kinases. We report here the crystal structure of APH, trapped in an inactive conformation by a tailor-made inhibitory ankyrin repeat (AR) protein, at 2.15 Å resolution. The inhibitor was selected from a combinatorial library of designed AR proteins. The AR protein binds the C-terminal lobe of APH and thereby stabilizes three α helices, which are necessary for substrate binding, in a significantly displaced conformation. BIAcore analysis and kinetic enzyme inhibition experiments are consistent with the proposed allosteric inhibition mechanism. In contrast to most small-molecule kinase inhibitors, the AR proteins are not restricted to active site binding, allowing for higher specificity. Inactive conformations of pharmaceutically relevant enzymes, as can be elucidated with the approach presented here, represent powerful starting points for rational drug design.

Introduction

Bacteria have developed a variety of pathways and mechanisms by which to inactivate antibiotics. Aminoglycosides, including kanamycin, amikacin, and streptomycin, are widely used in hospital care today, and, therefore, bacterial resistance to these antibiotics is a major concern in the health care field (Boehr et al., 2003). In general, aminoglycosides interact with the bacterial ribosome, thereby disrupting protein synthesis of the target cell. One way by which resistance to aminoglycosides can be achieved is by phosphorylation of hydroxy groups of the antibiotic. The aminoglycoside phosphotransferase (3′)-IIIa (APH) is a prototype enzyme for this mechanism (Boehr et al., 2001). It was found to mediate aminoglycoside resistance in *Enterococci* and *Staphylococci*. The crystal structure of APH has been determined (Hon et al., 1997), followed by a very detailed functional and structural analysis of the enzymatic mechanism (Thompson et al., 1999, 2002; Boehr et al., 2001; Burk et al., 2001). The fold of APH is structurally homologous to the catalytic domain of the eukaryotic Ser/Thr/Tyr protein kinases (EPKs; for example, the mitogen-activated protein kinase p38 [Wang et al., 1997], the insulin receptor kinase [Hubbard et al., 1994], or the Abelson tyrosin kinase [ABL] [Schindler et al., 2000]). It was concluded that APH and EPKs share a common ancestor, which suggests that APH is an ideal model system for all kinases sharing this fold (Hon et al., 1997).

EPKs are of great biological and medical importance because of their fundamental role in signal transduction and regulatory pathways in eukaryotic cells. Diseases, including cancer, inflammation and diabetes, are often directly linked to the malfunctioning of EPKs (Noble et al., 2004). The human genome encodes a total of 518 kinases (Manning et al., 2002). The highly conserved catalytic domain of kinases consists of an N-terminal, mostly β sheet-containing lobe and a C-terminal, α-helical lobe. The ATP binding pocket is located in the groove between the two lobes. Most of the known EPK inhibitors bind in the conserved ATP binding site, and a degree of specificity is only achieved by making use of small individual differences in the ATP binding pockets. This often leads to cross-reactivity and unwanted side effects of EPK inhibitors (Noble et al., 2004). Alternative inhibition mechanisms, not directly or exclusively targeting the active site, have proven to be highly efficient, albeit very hard to achieve. A prime example is the drug Gleevec, which only partially binds in the ATP pocket and inhibits ABL by stabilizing an inactive conformation of the kinase (Schindler et al., 2000).

We have developed proteinaceous APH inhibitors based on designed ankyrin repeat (AR) proteins (Amstutz et al., 2005). Designed AR proteins (Binz et al., 2003; Forrer et al., 2003, 2004) are built from single 33 amino acid repeat modules, which stack together to form elongated protein domains (Sedgwick and Smerdon, 1999). Molecules selected from designed AR protein libraries have been shown to bind different target proteins with high affinity and specificity (Binz et al., 2004). Furthermore, AR proteins are highly stable, well-expressed, and do not contain disulfide bonds, allowing for intracellular applications. The selected APH inhibitors (Amstutz et al., 2005) inhibit the enzyme both in vitro and in vivo and confer kanamycin and amikacin sensitivity to a level comparable to the gene knockout.

Here, we describe the crystal structure of APH in complex with one of the most potent AR protein inhibitors, AR_3a, to 2.15 Å resolution. It shows that the AR protein binds to the C-terminal lobe of APH outside the substrate binding pocket and stabilizes a significantly altered APH conformation with a distorted active site. Based on the structural data combined with the kinetic measurements, we suggest an allosteric inhibition mechanism. A comparison to other known allosteric protein kinase inhibitors reveals similarities and differences in the inhibition mechanism.

*Correspondence: gruetter@bioc.unizh.ch (M.G.G.); plueckthun@bioc.unizh.ch (A.P.)

[2]These authors contributed equally to this work.

Table 1. Statistics of the Data Collection and Refinement of the mAPH/AR_3a Complex

Data Collection	
Space group	$P2_1$
Cell dimensions, Å	a = 59.67, b = 98.08, c = 81.30 α = γ = 90.0, β = 110.01
Resolution limits, Å	20.0–2.15
Observed reflections	total: 163,030; unique: 46,440
Completeness, %	97.2 (81.0)[a]
Redundancy	3.5
R_{sym} (% on I)	5.3 (34.7)[a]
Wilson B factor, Å^2	45.0
Refinement	
Resolution range, Å	20.0–2.15
R factor/R_{free}, %	19.9/26.0
Ordered water molecules	353
Rms deviation from ideal geometry	
Bond lengths, Å	0.016
Bond angles, °	1.55
Average B factor, Å^2	52.8

[a] Numbers in parentheses refer to the highest-resolution shell.

Results and Discussion

Structure Determination and Overall Structure of mAPH/AR_3a Inhibitor Complex

To obtain crystals of APH in complex with the selected AR protein inhibitor, AR_3a, a mutant APH (mAPH) was created in which the two surface cysteine residues (C19, C156) of APH were replaced by serine. In wild-type APH (wtAPH), both cysteines can form intermolecular C19-C156 disulfide bonds, which mediate the formation of a homodimer in vitro (Hon et al., 1997). The protein complex mAPH/AR_3a was purified and crystallized in the presence of ATP, and X-ray diffraction data to 2.15 Å resolution were collected as described in Experimental Procedures. The structure was determined by molecular replacement by using wtAPH (Hon et al., 1997) and the designed AR protein E3_5 (Kohl et al., 2003) as search models (see Experimental Procedures). The final model of the mAPH/AR_3a enzyme inhibitor complex has an R factor of 19.9% and an R_{free} of 26.0% (Table 1 and Experimental Procedures).

Even though the protein is inactive in the complex with the AR protein (see below), the overall fold of mAPH is very similar to the one seen in all wtAPH structures (Hon et al., 1997), and it has structural homology to EPKs (see Figure 1). Between the N-terminal lobe, consisting mainly of β sheets, and the C-terminal, mostly α-helical lobe, there is a deep cleft harboring the ATP binding site (Figure 2A). The substrate binding pocket is adjacent to the ATP binding site and is formed mainly by the C-terminal, α-helical lobe. The AR protein inhibitor AR_3a with the typical AR domain fold (Kohl et al., 2003) binds to the α-helical lobe of mAPH. The conformation of this C-terminal lobe differs significantly from the one seen in structures of wtAPH alone. Strikingly, AR_3a binds the C-terminal lobe of mAPH on the opposite side as compared to the substrate (Figure 2A).

mAPH/AR_3a Conformations in the Asymmetric Unit

The asymmetric unit of the mAPH/AR_3a complex crystals contains two full heterodimeric complexes, named AB and CD. A and C represent mAPH molecules, whereas B and D represent AR_3a proteins. In the crystal, mAPH forms a pseudodimer, in which the molecules are related by a non-perfect 2-fold axis (150° rotation; 10° tilt) (Figure 2B) instead of the perfect 2-fold axis in the wtAPH structure (Figure 2C). The pseudodimer contacts cover about 1350 Å^2 buried accessible surface area (ΔASA) per mAPH (Table 2). However, wtAPH and mAPH employ the same set of residues to form the dimer interface (Figures 2B and 2C). The two heterodimeric complexes, AB and CD, exhibit different conformations (Figure 2D). A comparison of the structures of the A and C mAPH molecules with wtAPH reveals that molecule A has a higher similarity to wtAPH than does molecule C. In addition, molecule C has a distorted ATP binding site with the side chains Glu24, Gly25, and Met26 oriented differently. It also shows only weak electron density for the bound ADP at the position of the β phosphate and for the coordinating second Mg^{2+} ion. In contrast, the ATP binding site in molecule A is identical to that of wtAPH. The APH/AR_3a interface of complex AB displays 12 defined H bonds, compared to only 7 in the CD complex (Table 2 and Tables S1 and S2 in the Supplemental Data available with this article online). Therefore, the AB complex is better suited for the following analysis of the structure. The different conformations of APH in the crystal indicate that APH can adopt several different conformations, a phenomenon well known for EPKs (Huse and Kuriyan, 2002; Ozen and Serpersu, 2004).

mAPH/AR_3a Complex Structure

In the following section, we analyze the structure of mAPH, AR_3a, and the mAPH/AR_3a complex in detail. While the global fold of mAPH is conserved, the main differences in the mAPH structure, compared to wtAPH, are located in the AR_3a binding region, including mainly α helices A and B (Figures 1 and 3; see below) and the adjacent aminoglycoside positioning loop. In the wtAPH homodimer, this loop forms part of the dimer interface, which is stabilized in the crystal by two intermolecular disulfide bridges located on β strand one (C19) and on the aminoglycoside positioning loop between α helices A and B (C156). These disulfide bonds probably form only upon isolation of the protein, as this is a cytoplasmatic enzyme. In mAPH, with these cysteines mutated to serine, dimer formation in this region is not observed, and the aminoglycoside positioning loop is much more flexible and probably more similar to the situation seen in solution. In the mAPH-A molecule, this loop could not be modeled due to missing electron density for residues 149–166 (Figure 2A). In the mAPH-C molecule, electron density is visible for this section, but it is not continuous throughout the loop. Interestingly, in the dimeric wtAPH structure, the aminoglycoside positioning loop adopts a short α-helical conformation, whereas in the mAPH-C molecule, a short antiparallel β sheet is formed instead. These results demonstrate the high flexibility for the aminoglycoside positioning loop of monomeric APH in solution.

Superposition of molecules B and D (AR_3a molecules) with the designed AR protein E3_5 (Kohl et al.,

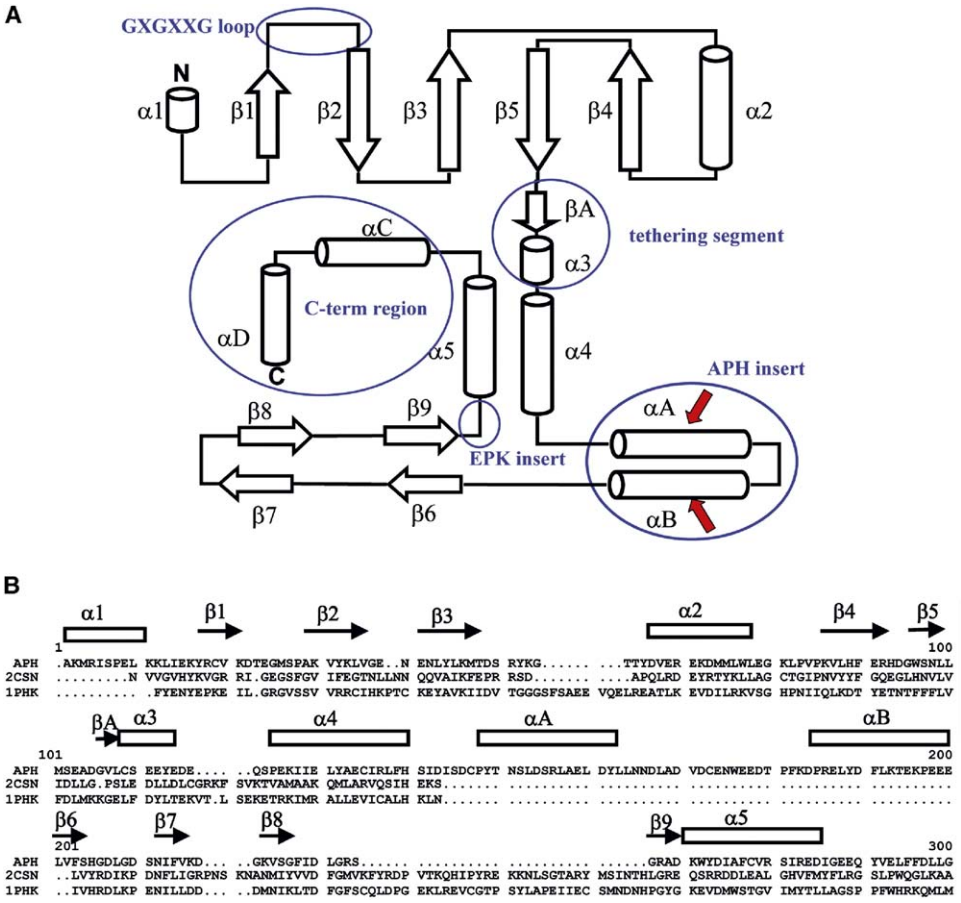

Figure 1. Topology and Structural Alignment of APH and Eukaryotic-Type Protein Kinase

(A) Topological diagram of APH and comparison with Eukaryotic-Type Protein Kinases (EPK). The contact regions between the APH molecule and the ankyrin repeat protein are indicated with red arrows. Blue circles indicate differences in folding between APH and EPK.

(B) Structural alignment between APH and two EPK representatives: the catalytic domain of casein kinase-1 (2CSN) and the catalytic domain of the phosphorylase kinase (1PHK). The C-terminal region of APH after helix α5 bears no resemblance to those seen in EPK's and therefore is not shown in the alignment. (Figure derived from [Hon et al., 1997]).

2003) and the maltose binding protein binder off7 (Binz et al., 2004) reveals virtually identical structures ($rmsd_{C\alpha} \leq 1.5$ Å, Figure 3F). The main differences occur in the C-terminal capping repeat of AR_3a, where weak electron density and high B factors were observed.

The protein-protein interaction surface of the APH/AR_3a complexes was analyzed by the same methods as those previously described (Binz et al., 2004). The analysis revealed a protein-protein interaction interface with global parameters highly comparable to other known AR protein-target protein complexes and other heterodimeric protein-protein interfaces (Lo Conte et al., 1999). The buried accessible surface area (ΔASA) on the AR_3a in the AB complex covers 850 $Å^2$, with 12 H bonds located in the interface (Table 2). Even though there are some differences found in the AB versus CD complex (Table 2), the interacting residues are highly conserved (Tables S1 and S2). The main hydrophobic contacts and six H bonds are formed by the same set of amino acids in both interfaces (Table 2). With 950 $Å^2$ ΔASA, the interaction surface of the AR_3a in the CD complex is even slightly larger than in the AB heterodimer. The differences in the protein-protein interaction result from the different crystal packing for the two heterodimers in the asymmetric unit, as discussed above.

Structural Differences of Free and Inhibited APH

On the mAPH (A and C) surface, mainly residues in α helices A and B are involved in the interaction with the AR protein (Tables S1 and S2). On the AR_3a surface, the interaction residues are located on the N-terminal capping repeat and on repeat modules 1, 2, and 3. While the fold of the AR protein is not affected by the binding (Figure 3F), the structure of mAPH is significantly distorted locally (Figures 3A–3C). α helices A and B in the mAPH model are shifted by 5–7 Å in comparison to the wtAPH structure (Figures 3B and 3C). In addition, α helix B is rotated by 45°–90°, depending on which reference point is chosen (Figure 3C). For example, Tyr172 is partially buried and is only slightly exposed to the solvent in the wtAPH structure, whereas in the mAPH/AR_3a complex, it is involved in the protein-protein interaction with the AR protein and is rotated by

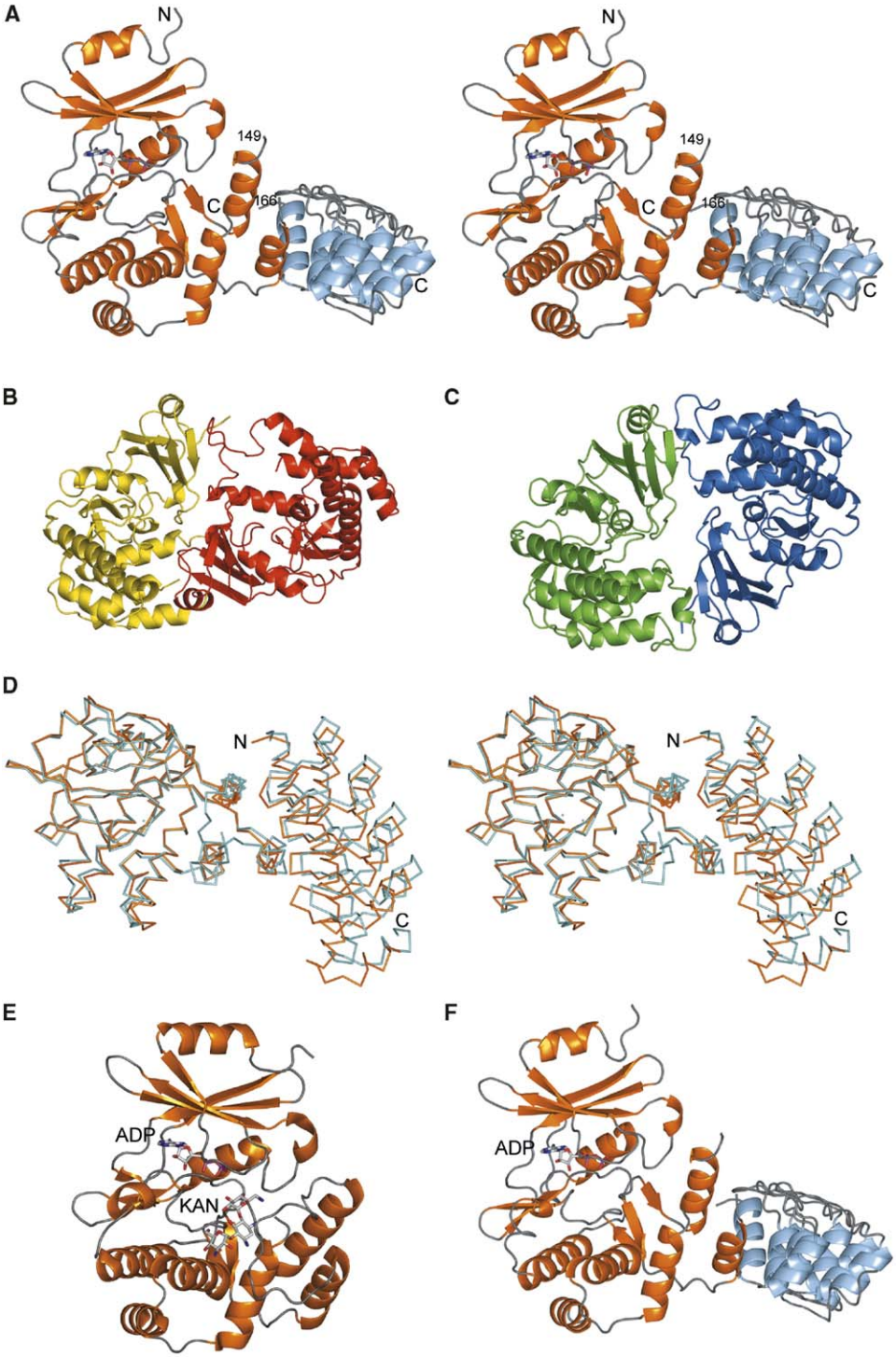

Figure 2. Crystal Structure of the mAPH in Complex with the AR Protein AR_3a

(A) Stereo view of the AB heterodimer of the mAPH/AR_3a complex. The mAPH is shown in orange, and the AR_3a is shown in light blue. AR_3a binds to the C-terminal lobe of the mAPH and stabilizes an inactive conformation.

(B) Asymmetric mAPH pseudo-homodimer found in the crystal of the mAPH/AR_3a complex.

(C) Symmetric wtAPH dimer found in the wtAPH crystal.

(D) Stereo view of the superposition of the mAPH hetereodimer AB (orange) and BC (light blue).

(E) wtAPH in the kanamycin A bound form (PDB: 1L8T). ADP and kanamycin A are labeled.

(F) mAPH/AR_3a AB heterodimer in the same orientation as the wtAPH in (E).

Table 2. Comparison between AR Protein Target Complexes and Other Protein-Protein Interactions

PDB ID[a]	Resolution (Å)	ΔASA[b] (Å^2)	Number of H Bonds	Number of H Bonds/ 100 (Å^2) ΔASA[b,c]	Number of Salt Bridges[c]	Planarity[c]	Number of Bridging H_2O[c]
1awc	2.2	853.62	5	0.58	0	2.30	3
1bi7	3.4	1205.5	7	0.29	4	2.50	0
1blx	1.9	845.4	11	1.30	1	2.50	12
1g3n	2.9	843.3	12	1.42	1	2.20	0
1svx	2.3	611.2	6	1.00	0	2.10	0
APH/AR_3a, AB heterodimer	2.15	847.9	12	2.10	0	2.2	0
APH/AR_3a, CD heterodimer	2.15	950.6	7	0.73	0	2.0	0
APH, AC homodimer	2.15	1371.7	3	0.22	2	3.0	0
APH, CA homodimer	2.15	1367.6	3	0.22	2	3.0	0
Heterodimeric protein-protein complexes[c]	—	983 ± 582	—	1.1 ± 0.5	—	2.8 ± 0.9	—

[a] Protein Data Bank (PDB) accession code (Berman et al., 2000).
[b] Surface area per molecule occluded upon complex formation; if not stated otherwise, the AR protein is analyzed.
[c] According to Lo Conte et al. (1999).

almost 90°. In the wtAPH structure, α helix D is oriented through a number of contacts mainly formed with residues located on α helix B. As a consequence of the alteration of α helix B by AR_3a, α helix D is severely distorted, compared to the wtAPH conformation (see below).

In another recently determined crystal structure of the selected AR protein off7 in complex with maltose binding protein, no structural change of the target protein upon binding of the AR protein was observed (Binz et al., 2004). We therefore believe that APH has a malleable fold. We suggest that AR_3a traps APH in a con-

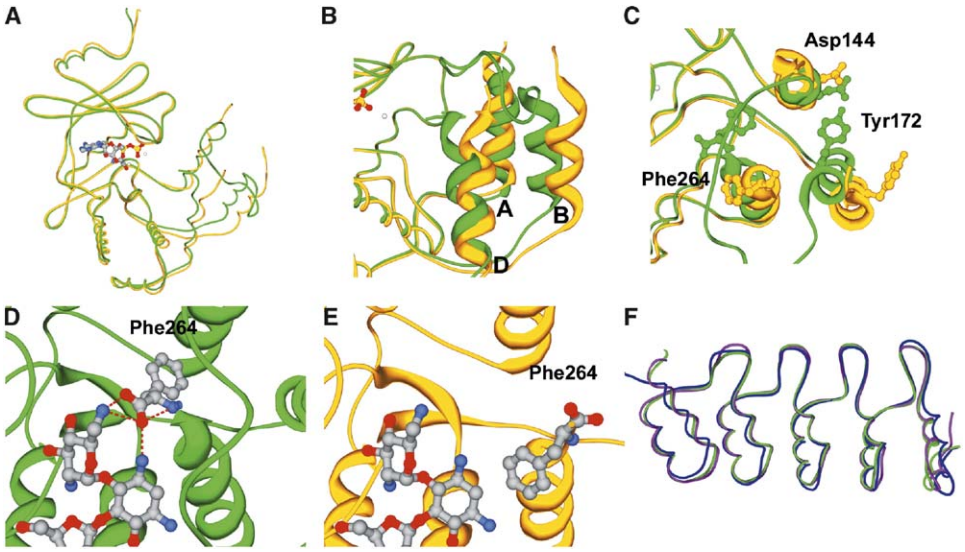

Figure 3. Superpositions and Comparison of wtAPH to mAPH/AR_3a

wtAPH is shown in green, and mAPH/AR_3a (AB heterodimer) is shown in yellow.

(A) Global superposition of the wtAPH structure and the mAPH.

(B) Closeup view of the α helices A, B, and D in the C-terminal lobes of the two APH molecules. The α helices A and B are involved in the interaction with the AR_3a. In mAPH/AR_3a, the α helix D is not held in position anymore by the contacts with α helices A and B. Instead, it is shifted by 5–7 Å with respect to the wtAPH structure.

(C) Closeup view of the α helices A, B, and D rotated by 90° around the horizontal axis with respect to the view in (B). To illustrate the changes in more detail, the side chains of Asp144, Tyr172, and Phe264 are displayed.

(D) Kanamycin A binding pocket in the wtAPH structure and H bonding to Phe264 on α helix D. Phe264 forms three H bonds to kanamycin A.

(E) Disrupted binding site of kanamycin A in the mAPH/AR_3a complex. The kanamycin A is modeled into the mAPH/AR_3a structure. Phe264 on α helix D is not capable of forming H bonds to kanamycin A anymore.

(F) Superposition of the AR proteins E3_5 (green), off7 (purple), and AR_3a (blue). In all three AR proteins, the global fold is unchanged, but local changes occur, especially in the N- and C-terminal capping repeats.

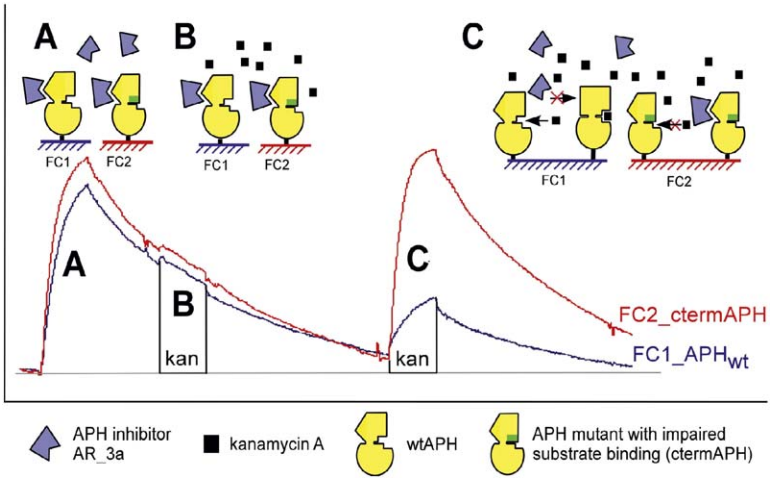

Figure 4. BIAcore Analysis of the Interaction of Inhibitor AR_3a to wtAPH and Inactive ctermAPH in the Presence and Absence of Kanamycin A

Equal amounts of wtAPH in flow-cell one (FC1) (blue) and of ctermAPH in flow-cell two (FC2) (red) were immobilized on a sensor chip. By the additional two C-terminal residues, the active site of ctermAPH is occluded (indicated by a green rectangle in the cartoon).

(A) Binding of the inhibitor was monitored in the absence of kanamycin A, showing comparable binding on both forms of APH.

(B) Addition of a pulse of kanamycin A (200 μM) during the washing procedure did not affect the off-rate of the inhibitor.

(C) Addition of kanamycin A (200 μM) during the binding phase reduced the binding of the inhibitor to the wtAPH, but did not affect the binding to the mutant ctermAPH, which does not bind kanamycin A.

formation that is less populated and perhaps present in solution.

BIAcore Analysis

To investigate whether the binding to kanamycin or to the AR inhibitor is mutually exclusive, the binding behavior of AR_3a to APH was characterized for its dependence on the presence of substrate by BIAcore experiments. The C-terminal amino acid Phe264 of wtAPH, in particular its terminal carboxy group, is essential for substrate binding, as mutations at this site drastically impair binding of substrate (Thompson et al., 1999). We constructed an APH mutant (ctermAPH) with two additional C-terminal amino acids (Gln, Ala). This mutant showed no kinase activity.

Similar amounts of both wtAPH and ctermAPH were immobilized on parallel flow cells on a BIAcore chip. Binding of AR_3a to wtAPH and ctermAPH was monitored in parallel. A pulse of 200 μM kanamycin A was applied either during the injection phase, showing the effect of kanamycin A on the association rate, or during washing, showing the kanamycin A effect on the dissociation rate (Figure 4). As expected, the association and dissociation of AR_3a to ctermAPH—which does not interact with kanamycin A—is identical in the presence or absence of kanamycin A. The association of AR_3a to wtAPH, however, is strongly reduced in the presence of kanamycin A (Figure 4). The apparent on-rate was reduced more than 150-fold in the presence of 100 μM kanamycin A (data not shown). The off-rate, on the other hand, was not influenced by kanamycin A (Figure 4). In conclusion, kanamycin A and AR_3a seem to compete for binding to wtAPH, albeit not for the active site, but rather for a malleable APH molecule that can assume different conformations. The dissociation of the APH/AR_3a complex occurs with a given rate, which seems not to be influenced by kanamycin A.

Inhibition

To further elucidate the mechanism of inhibition of the inhibitor AR_3a, in vitro inhibition studies were performed. wtAPH, AR_3a, and wtAPH/AR_3a complex were expressed and purified as described in Experimental Procedures. wtAPH purification resulted in a mixture of monomer and dimer as described previously (McKay et al., 1994). For the in vitro inhibition studies, only the isolated monomeric APH was used. Purified AR_3a protein tended to form a mixture of monomers, dimers, and multimers, which showed a fast equilibrium (Amstutz et al., 2005). This is a property of this particular inhibitor (Binz et al., 2003, 2004). The isolated wtAPH/AR_3a complex was investigated by size-exclusion chromatography and gave rise to a single peak with a 1:1 ratio (Amstutz et al., 2005).

The steady-state velocities of enzyme activity were monitored by coupling the release of ADP to a pyruvate kinase/lactate dehydrogenase reaction as described previously (McKay et al., 1994), with some modifications (see Experimental Procedures). We decided to use amikacin for these studies, as, with this substrate, APH follows simple Michaelis-Menten kinetics. This is in contrast to what is seen in kanamycin A, a case in which the analysis is complicated by substrate inhibition (Amstutz et al., 2005). Due to the nature of the coupled assay and the lack of knowledge of the exact molarity of the active species of both wtAPH and AR_3a, a quantitative analysis of the inhibition mechanism was not possible. Therefore, we focused on a qualitative investigation of the inhibition mechanism and give ranges of constants when possible.

For determining the binding mode, progress curves in the presence of wtAPH alone and wtAPH at various concentrations of the inhibitor AR_3a were analyzed. If the reaction was started with the enzyme, each curve with inhibitor present showed an initial exponential "burst" phase, followed by a slower steady-state rate after some minutes (data not shown). These curves suggest slow, tight binding inhibition. The association and dissociation rate constants (k_{on} = 1.6•10^6 M^{-1} s^{-1}, k_{off} = 2.7•10^{-3} s^{-1}) determined in BIAcore experiments (Amstutz et al., 2005) further support a tight binding mechanism with observable pre-steady-state kinetics in this range.

For the classification of the inhibition mechanism,

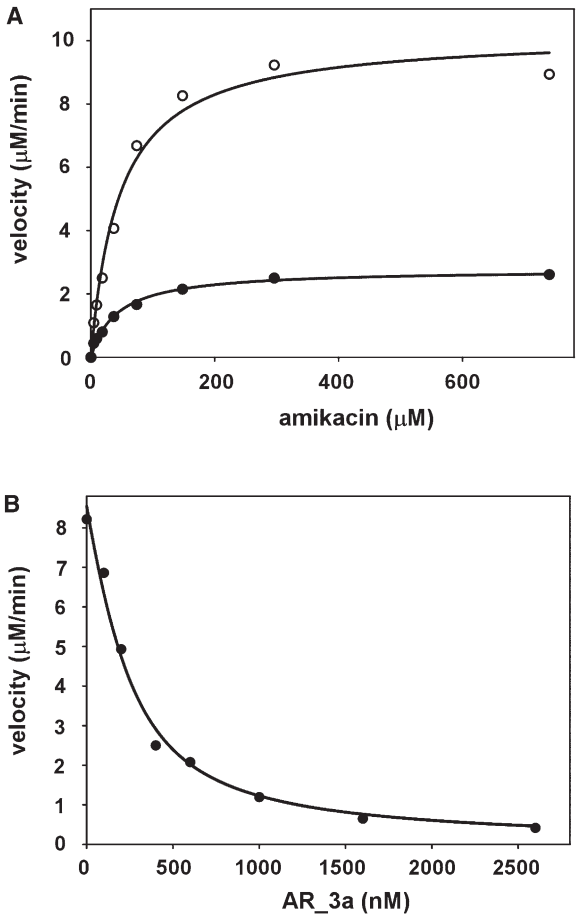

Figure 5. In Vitro Inhibition of wtAPH by AR_3a

(A) Enzyme activities of both wtAPH (open circles) and purified wtAPH/AR_3a complex (closed circles) were analyzed at various amikacin concentrations. The wtAPH/AR_3a complex shows a reduction of V_{max} with little effect on the K_m value.

(B) Amikacin phosphorylation by wtAPH was determined in the presence of various concentrations of the inhibitor AR_3a. Steady-state velocities were measured at 740 μM amikacin and were plotted as a function of inhibitor concentration. wtAPH seems to be completely inhibited by AR_3a. All assays were carried out at 20°C with 200 nM wtAPH or 200 nM equilibrated wtAPH/AR_3a complex.

steady-state velocities of wtAPH and wtAPH/AR_3a complex were determined at various substrate concentrations, and the steady-state velocities were plotted as a function of substrate concentration (Figure 5A). The rates were fitted by using the standard Michaelis-Menten equation. The K_m and V_{max} values determined for 200 nM wtAPH are 46.43 ± 7.16 μM and 10.22 ± 0.45 μM/min (corresponding to k_{cat} = 0.85 s^{-1}), respectively, and are 42.41 ± 4.63 μM and 2.78 ± 0.08 μM/min (corresponding to k_{cat} = 0.23 s^{-1}), respectively, for 200 nM equilibrated wtAPH/AR_3a complex. The wtAPH/AR_3a complex thus shows a reduction of V_{max} with little effect on the K_m value. This is in agreement with a mixed-type inhibition (Scheme 1), containing a competitive and an uncompetitive component. A purely uncompetitive inhibition, which would predict a lower apparent K_m, can furthermore be ruled out, because AR_3a also binds the free enzyme in BIAcore experiments (Figure 4). A purely competitive inhibition would not alter V_{max}. In Figure 5B, velocities of both wtAPH alone and in the presence of various concentrations of AR_3a were plotted as a function of inhibitor concentration. Inhibitor titration revealed that AR_3a completely inhibits the enzymatic activity of wtAPH in vitro. This is in agreement with the structural data, by which the substrate binding site is shown to be highly disordered upon inhibitor binding (see below). Virtually identical results were obtained with mAPH (data not shown), suggesting that the introduction of the two cysteine to serine mutations had no influence on the enzyme or on its inhibition by AR_3a.

For the determination of the inhibition constant αK_i, the data were fitted to the equation for tight binding conditions (Scheme 1; Szedlacsek et al., 1988) or directly with the model of Scheme 1 by DYNAFIT (Kuzmic, 1996). In either case, the αK_i value obtained was 140 ± 18 nM, with the α coefficient in the range of 1–3. Since the active species of enzyme and inhibitor could not be determined, a separate specification of K_i and α was not possible. Yet estimating α = 1–3 from the fit, the K_i obtained in the in vitro inhibition studies is 30–100 times higher than the K_D determined in BIAcore experiments (K_D = 1.7 nM; Amstutz et al., 2005). There are several contributing factors to this observation. First, in the BIAcore measurements, only the interaction between APH and AR_3a is investigated, whereas in the kinetic studies, the substrates amikacin and Mg•ATP are also present. The second reason might result from different assay conditions (different buffer composition) of the kinetic measurements. Third, overestimation of the concentration of active AR_3a molecules due to oligomerization (Amstutz et al., 2005) in the kinase buffer might have an effect on the observed inhibition constant.

Even though we cannot quantitatively determine the kinetic parameters, it is important to emphasize that these in vitro inhibition studies demonstrate that AR_3a completely inhibits APH (wtAPH and mAPH) by a mixed-type inhibition mechanism.

Inhibition Mechanism

Based on the structure of the complex and the in vitro data on inhibition and binding, we propose the following inhibition mechanism: the AR_3a inhibitor and the substrate compete for binding to APH. The conformation stabilized by the inhibitor is unproductive, while the one binding substrate is the active form of APH. The mixed-type inhibition seen kinetically (Figure 5A) suggests that the substrate can bind, albeit poorly, to the enzyme-inhibitor complex, EI; however, the complete inhibition at high inhibitor concentrations (Figure 5B) shows that the enzyme-substrate-inhibitor complex (ESI) is not catalytically active.

The reaction mechanism for the phosphorylation of kanamycin by wtAPH was analyzed in detail (Hon et al., 1997; Thompson et al., 1999, 2002; Boehr et al., 2001; Burk et al., 2001). It was shown that, among other residues, the very C-terminal amino acid Phe264 in α helix D is crucial for substrate binding (Figure 3D) (Thompson et al., 1999). The terminal carboxylate of Phe264 forms

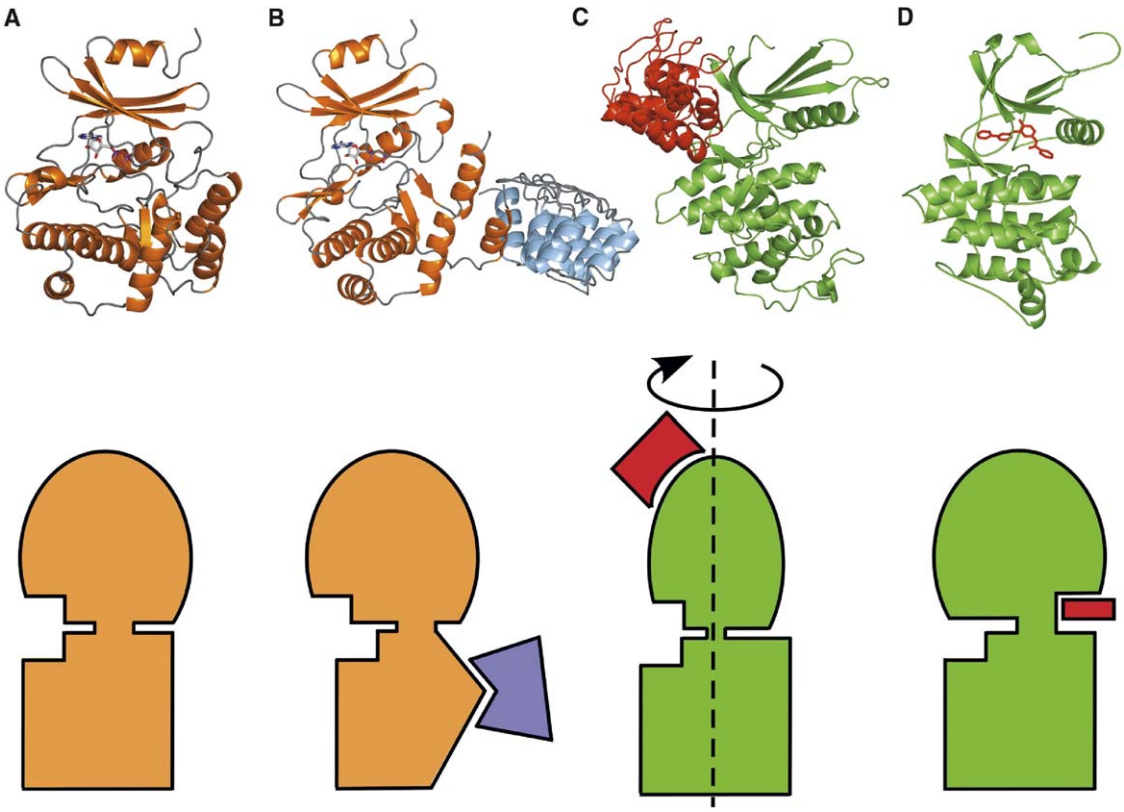

Figure 6. Structural Comparison of mAPH/AR_3a Structure to Other Inhibitor-Kinase Complexes

(A) The wtAPH monomer is shown in orange.

(B) mAPH/AR_3a structure (AB heterodimer) with mAPH, shown in orange, bound by AR_3a, shown in light blue. The AR protein binds to the C-terminal lobe of the kinase and distorts the kanamycin A binding site.

(C) Cyclin-dependent kinase 6 shown in green, bound by AR protein p18, shown in red. p18 binds to the N-terminal lobe and distorts residues in the ATP binding pocket, altering the binding surface for the cyclin substrate.

(D) Crystal structure of the Abelson tyrosine kinase, shown in green, and the inhibitor STI-571 (Gleevec), shown in red. STI-571 stabilizes an inactive conformation of ABL, in which the central activation loop remains unphosphorylated; therefore, the kinase is inactive.

three H bonds to the substrate and thus orients the aminoglycoside in the active site. Point mutations or deletions of Phe264 turned out to have a drastic effect on the enzymatic activity, impairing the binding of kanamycin to APH and thus inhibiting the enzyme (Thompson et al., 1999). In the mAPH/AR_3a complex, we observe that, by binding of the AR protein to mAPH, α helices A and B are oriented differently than in the wtAPH structure. In the wtAPH structure, the α helices A and B and the aminoglycoside positioning loop are needed to form a shell that positions the C-terminal α helix D. In the inhibited mAPH/AR_3a complex, this shell is removed and α helix D is much more flexible. This leads to a shift of up to 7 Å and a movement of the C-terminal α helix D (Figures 3B and 3E). As a consequence, the terminal carboxylate of Phe264 cannot form the essential H bonds with kanamycin anymore, finally resulting in enzyme inhibition (Figure 3E). The inhibition data are in agreement with the effects seen for Phe264 point mutations and deletions (Thompson et al., 1999) and also confirm the inactivity of the mutant extended by two amino acids (data not shown). BIAcore experiments demonstrate that kanamycin A, which interacts with the terminal carboxylate of Phe264, stabilizes a conformation, which is only poorly recognized by AR_3a. All results indicate that inhibition of APH is achieved through stabilization of an inactive conformation of APH by AR_3a.

Comparison to Other AR Protein Kinase Inhibitors and Gleevec: Implications for Drug Design and Cell Biology

Natural AR proteins are well known as regulators and inhibitors of kinases. Several crystal structures of the cyclin-dependent kinase 6 (Cdk6) with different AR protein inhibitors of the INK4 family (p16, p18, and p19) illustrate an allosteric inhibition mechanism (Russo et al., 1998; Brotherton et al., 1998; Pavletich, 1999; Jeffrey et al., 2000). Upon binding of the AR protein, a conformational change occurs in Cdk6. The N-terminal lobe of Cdk6 rotates by 10°–15°, leading to a misalignment of residues needed to bind ATP and to a conformational change in the interface needed for the binding of cyclin (Figure 6C), which in turn is needed to activate the kinase. The AR proteins p16, p18, and p19 bind mainly to the N-terminal lobe of Cdk6, at the back of the ATP binding cleft. The inhibition mechanism seen in the mAPH/AR_3a complex is remarkably similar, even though the AR protein binds to a different part of the protein. The binding of AR_3a to the C-terminal lobe of

APH induces a structural change in the substrate binding site, leaving the ATP binding pocket unchanged, but resulting in an inhibited APH (Figures 6A and 6B).

As shown here and in Amstutz et al. (2005), selected AR protein inhibitors for kinases are highly specific and do not need to target the ATP binding site for inhibition, but exploit "natural" conformational fluctuations of kinases. Most conventional small-molecule kinase inhibitors target the ATP binding pocket and act as competitive inhibitors to ATP. As this site is highly conserved, specificity is difficult to achieve (Noble et al., 2004). For example, inhibition of APH by some EPK inhibitors has been described (Daigle et al., 1997). This emphasizes the structural homology of APH and EPKs, especially for the ATP binding site. It also demonstrates the poor specificity of these EPK inhibitors. For human EPKs involved in diseases, specificity is absolutely required. Unspecific binding of inhibitors to several EPKs can cause severe side effects and can prevent their pharmaceutical use (Noble et al., 2004).

The Abelson tyrosine kinase (ABL) inhibitor ST1-571 (Gleevec) binds to the N-terminal lobe of ABL and in the ATP binding pocket, and thereby traps the kinase in an inactive conformation, with its activation loop bound back into the peptide binding cleft (Figure 6D; Schindler et al., 2000). This prevents the phosphorylation of the binding loop and thus the activation of ABL kinase. So far, targeting such an inactive form of a kinase was a pure trial-and-error process and relied on high-throughput screening (Noble et al., 2004). The structure presented here, and especially the approach via the selection of specific protein-based inhibitors, could open new opportunities in the structure-based drug design (Anderson, 2003). The mAPH/AR_3a crystal structure showing a nonproductive kinase conformation, and similar studies for other EPKs, could serve as a starting point for structure-based drug design of APH and other kinase inhibitors. In principle, the same approach of using selected AR protein inhibitors for cocrystallization could also be applied to EPKs. In fact, pools of binders to JNK2 and p38 have already been selected, and the binding of some individual binders has been characterized (Binz et al., 2004). The pools of binders could act as a starting point for inhibitor screens, followed by cocrystallization of identified inhibitor/enzyme complexes. Subsequent structure-based drug design might allow for the development of highly specific drugs. This approach is not at all limited to kinases, and it might be applied to any other enzyme.

In a cell, kinases are not only regulated by direct activation or inactivation, but they are regulated by their localization as well (their interplay with other kinases, their corresponding phosphatases, and other regulating proteins [Sharrocks et al., 2000]; [Enslen and Davis, 2001]; [Pawson and Nash, 2003]; [Tanoue and Nishida, 2003]). Amstutz et al. (2005) showed that AR proteins can be used intracellularly as well as extracellularly, providing a similar phenotype as a knockout mutant. Therefore, AR proteins may also interfere in signaling cascades of kinases or in other pathways. It can be easily envisioned that the binding of a selected AR protein can prevent the docking of the kinase to the scaffolding protein, the interaction with a phosphatase, or the interaction with an upstream activating kinase. The possibility of preventing specific interactions with a selected AR protein would offer individual researchers many novel possibilities to design their experiments and has several advantages over conventional methods used so far (for a more detailed discussion, see [Amstutz et al., 2005]).

Experimental Procedures

Cloning and Production of Proteins

Biotinylated wtAPH was produced as described in Amstutz et al., (2005). A biotinylated mutant of APH (ctermAPH), carrying two additional amino acids at the C terminus (Gln, Ala), was constructed and produced as described for the biotinylated wtAPH (Amstutz et al., 2005), with the sole difference that the reverse primer for the PCR of the APH gene was APHmutCTr (5′-TACTCAAGCTTGAAA CAATTCATCCA-3′). For the construction of the untagged double cysteine to serine mutant (mAPH), in which cysteines 19 and 156 of APH were mutated to serines, the mutations were introduced by PCR. The mAPH gene was inserted into pQE60 (Qiagen, Hilden, Germany) without a tag and expressed in *E. coli* XL-1Blue, as described for the AR proteins (Binz et al., 2003, Kohl et al., 2003). APH variants (wtAPH, mAPH, ctermAPH) were purified by using a 25 ml Q-Sepharose column (Amersham Pharmacia, Dübendorf, Switzerland), followed by preparative Superdex-75 (Amersham Pharmacia) size-exclusion chromatography in 10 mM HEPES (pH 7.5), 100 mM NaCl, 50 mM $MgCl_2$, and 2 mM dithiothreitol (DTT), according to the published protocol (Hon et al., 1997). Only fractions corresponding to the monomeric APH were used for subsequent experiments. For BIAcore and inhibition experiments, the APH inhibitor AR_3a was expressed and purified as described (Binz et al., 2003, Kohl et al., 2003).

mAPH/AR_3a Complex

wtAPH, mAPH, and the selected APH inhibitor AR_3a were expressed as described above. The cell pellets of 1 l bacterial culture of APH and AR_3a were resuspended and combined in 30 ml buffer (50 mM HEPES [pH 7.5], 200 mM NaCl, 10 mM $MgCl_2$). The cells were lysed by using an Emulsiflex C5 (Avestin, Ottawa, ON, Canada) with the addition of Complete Protease Inhibitor (Roche, Basel, Switzerland) and DNaseI (Roche). The cell debris was pelleted by centrifugation at 50,000 × g for 30 min at 4°C. The resulting supernatant was applied to an immobilized metal-ion affinity chromatography column (Qiagen), equilibrated with 50 mM HEPES (pH 7.5), 200 mM NaCl, 20 mM imidazole, 10 mM $MgCl_2$. After extensive washing with equilibration buffer, the complex was eluted with 50 mM HEPES (pH 7.5), 200 mM NaCl, 250 mM imidazole, 10 mM $MgCl_2$ and was further purified by preparative Superdex-75 (Amersham Pharmacia) size-exclusion chromatography in 10 mM HEPES (pH 7.5), 100 mM NaCl, 50 mM $MgCl_2$, and 3 mM DTT. The peak fraction with the expected molecular weight of the complex, containing one of the APH variants and AR_3a in equimolar amounts (determined by SDS-PAGE), was collected and used for further experiments. Dynamic light scattering of these fractions was measured as described (Kohl et al., 2003) and showed a monodisperse distribution for both complexes.

Crystallization

The mAPH/AR_3a complex was concentrated to 10–12 mg/ml, and 5 mM ATP (pH 7.0) was added. Initial crystallization screening was done by using a four channel Lissy (Zinsser, Germany) liquid handler for pipetting the reservoir and a Cartesian eight channel MicroSys (Zinsser) system for the sitting drop setup. As a default, 100 μl reservoir solution was used in combination with 100 nl protein solution, added to 100 nl reservoir solution in 96-well sitting drop CrystalQuick round well crystallization plates (Greiner Bio-One, Frickenhausen, Germany). The initially obtained crystals were refined by using standard techniques in a 1 μl + 1 μl setup. The crystals used for data collection were grown in 1–3 days in 15%–20% PEG 5500, 0.1 M Mes/HCl (pH 5.9–6.2). For cryoprotection, 10% ethylene glycol was employed.

Data Collection, Reduction, Structure Solution, and Refinement

Data of single crystals were collected at the Swiss Light Source biocrystallography beamline (Villigen, Switzerland). The data were processed with DENZO, SCALEPACK, and TRUNCATE (Otwinowski and Minor, 1997). The crystal belonged to space group $P2_1$, with a Matthews coefficient V_M of 2.1 $Å^3$/Da, corresponding to an estimated water content of 41%.

The crystal structure was determined by molecular replacement by using the program AMoRe (Navaza, 1994, 2001), with the structure of the unselected N3C library member E3_5 (PDB-ID 1MJ0 [Kohl et al., 2003]) and a monomeric APH model (PDB-ID 1J7L) used as search models. First, we applied a conventional AMoRe protocol with a wtAPH monomer as a search model. This yielded two solutions for mAPH with only very little additional density for a potential AR protein and no success in further refinement. An AMoRe search with the AR protein E3_5 as a search model did not yield a meaningful solution. The program AMoRe offers the possibility to apply an n-body translational search, which is routinely used in AMoRe, but usually only with one search model. Here, we applied a modified protocol for an n-body search with two search models. Two separate structure factor tables, followed by separate rotational searches for each of the two search models, were calculated from APH (1J7L) and from the AR protein (1MJ0). A conventional translational search was applied for a first APH molecule, which led to a clear solution. This solution was fixed, and the translational search was repeated for a second APH molecule, leading to a second solution, which was again fixed. In the next step, the structure factor table and the rotational search list of the AR protein E3_5 were used in a translational search in combination with the already fixed solutions for the APH, now yielding a solution for the AR protein. A second search with two fixed APH molecules and one fixed AR protein failed to give a solution distinguishable from the background for a second AR protein. However, in the electron density derived, using the phases of two APH and one AR protein, clear additional density was seen for a second AR protein. The second AR protein was modeled into the density with the program O (Jones et al., 1991). Subsequent refinement with CNS (Brünger et al., 1998), REFMAC (Murshudov et al., 1999), the CCP4 program suite (CCP4, 1994), and, for the model building, O (Jones et al., 1991) resulted in a final model with an R factor of 19.9% and an R_{free} of 26.0%, Table 1.

Analysis of the Complexes

The structural analysis of the complexes was done as suggested by Jones and Thornton (1996) and as described previously (Binz et al., 2004).

Surface Plasmon Resonance

SPR was measured with a BIAcore3000 instrument (BIAcore, Uppsala, Sweden). The running buffer was 20 mM HEPES (pH 7.4), 150 mM NaCl, 10 mM $MgCl_2$, 1 mM DTT, 0.005% Tween 20. An SA chip (BIAcore) was used with about 500 RU biotinylated pD_APH immobilized on flow cell 1 and about 450 RU biotinylated pD_ctermAPH on flow cell 2. AR_3a was applied at a concentration of 200 nM either in running buffer or in running buffer with 200 μM kanamycin A. After application of AR_3a in the absence of kanamycin A, a pulse of 150 μl running buffer containing 200 μM kanamycin A was injected during dissociation (for details, see Figure 4). On- and off-rates in the presence of 100 μM kanamycin A were measured at a flow of 50 μl/min with 5 min buffer flow, a 2 min injection of AR_3a in varying concentrations (10, 50, 100, 200, 500, 1000 nM), and an off-rate measurement of 40 min with buffer flow. The signal of an uncoated reference cell was subtracted from the measurements. The kinetic data of the interaction were evaluated by using the software BIAevaluation 3.0 (BIAcore).

Enzyme Assay

APH activity was monitored by coupling the production of ADP to the consumption of NADH in a pyruvate kinase/lactate dehydrogenase (PK/LDH) reaction as described (McKay et al., 1994), with some modifications (Amstutz et al., 2005). 990 μl assay buffer (50 mM HEPES [pH 7.5], 10 mM $MgCl_2$, 40 mM KCl, 160 mM NaCl, 5U PK, 5U LDH, 2.5 mM phosphoenolpyruvate, 0.025% BSA, 0.12 mg/ml NADH, 1 mM ATP) containing either 200 nM purified wtAPH or wtAPH/AR_3a complex (1:1) was added in a 10 mm QS cell (HELLMA, Basel, Switzerland). The mixtures were preincubated for 15 min, and the assay was initiated by addition of 10 μl of different amikacin concentrations (Sigma, A1774). Both the preincubation and the assay were carried out at 20°C. The oxidation of NADH was followed by continuously monitoring the absorbance at 340 nm. The steady-state rates were normalized for background activity by subtracting the activity monitored in the absence of amikacin. Velocities were plotted as a function of the substrate concentration. The data were fitted to the standard Michaelis-Menten equation to determine V_{max} and K_m values.

For the analysis of the inhibition constant, the kinetic measurements were carried out with 200 nM wtAPH or wtAPH in complex with various amounts of inhibitor AR_3a. For the formation of complexes, 35 μM wtAPH was mixed with AR_3a in a molar ratio of 1:0.5 to 1:13 and was incubated for 2 hr at 4°C prior to the dilution (1:175) in the enzyme assay. The reaction was started with 740 μM amikacin. Enzyme activities were plotted as a function of the inhibitor concentration, and the data were fitted by the general equation for tight binding inhibition based on the mechanism in Scheme 1 (Szedlacsek et al., 1988).

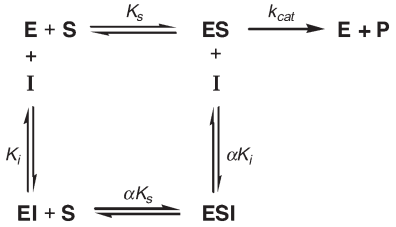

Scheme 1.

In this scheme, E is the enzyme, S represents the substrate, P represents the product, and I represents the inhibitor. K_S = [E][S]/[ES], K_i = [E][I]/[EI], αK_S = [EI][S]/[ESI], αK_i = [ES][I]/[ESI], k_{cat} = catalytic constant, and α is a coefficient. The αK_i value was determined to 140 ± 18 nM with the α coefficient in the range of 1–3.

Supplemental Data

Supplemental Data including the accessible surface area per residue buried and the hydrogen bonds formed in the APH/AR_3a complex are available at http://www.structure.org/cgi/content/full/13/8/1131/DC1/.

Acknowledgments

We would like to thank Sandra Lepthien, Maya Gulotti, and Beat Blattmann for help in protein preparation and crystallization and the members of the Plückthun and Grütter laboratories for valuable discussions. We would also like to thank Prof. Antonio Baici for his help and discussion on APH kinetics. H.K.B. was supported by a predoctoral fellowship of the Roche Research Foundation. This work was supported by the Swiss National Center of Competence in Research (NCCR) in Structural Biology and the Swiss Krebsliga.

Received: February 17, 2005
Revised: April 25, 2005
Accepted: April 26, 2005
Published: August 9, 2005

References

Amstutz, P., Binz, H.K., Parizek, P., Stumpp, M.T., Kohl, A., Grütter, M.G., Forrer, P., and Plückthun, A/ (2005). Intracellular kinase inhibitors selected from combinatorial libraries of designed ankyrin repeat proteins. J. Biol. Chem. *280*, 24715–24722.

Anderson, A. (2003). The process of structure-based drug design. Chem. Biol. *10*, 787–797.

Berman, H.M., Westbrook, J., Feng, Z., Gilliland, G., Bhat, T.N.,

Weissig, H., Shindyalov, I.N., and Bourne, P.E. (2000). The Protein Data Bank. Nucleic Acids Res. *28*, 235–242.

Binz, H.K., Stumpp, M.T., Forrer, P., Amstutz, P., and Plückthun, A. (2003). Designing repeat proteins: well-expressed, soluble and stable proteins from combinatorial libraries of consensus ankyrin repeat proteins. J. Mol. Biol. *332*, 489–503.

Binz, H.K., Amstutz, P., Kohl, A., Stumpp, M.T., Briand, C., Forrer, P., Grütter, M.G., and Plückthun, A. (2004). High-affinity binders selected from designed ankyrin repeat protein libraries. Nat. Biotechnol. *22*, 575–582.

Boehr, D.D., Thompson, P.R., and Wright, G.D. (2001). Molecular mechanism of aminoglycoside antibiotic kinase APH(3′)-IIIa. Roles of conserved active site residues. J. Biol. Chem. *276*, 23929–23936.

Boehr, D.D., Draker, K., Koteva, K., Bains, M., Hancock, R.E., and Wright, G.D. (2003). Broad-spectrum peptide inhibitors of aminoglycoside antibiotic resistance enzymes. Chem. Biol. *10*, 189–196.

Brotherton, D., Dhanaraj, V., Wick, S., Brizuela, L., Domaille, P., Volyanik, E., Xu, X., Parisini, E., Smith, B., Archer, S., et al. (1998). Crystal structure of the complex of the cyclin D-dependent kinase Cdk6 bound to the cell-cycle inhibitor $p19^{INK4d}$. Nature *395*, 244–250.

Brünger, A.T., Adams, P.D., Clore, G.M., DeLano, W.L., Gros, P., Grosse-Kunstleve, R.W., Jiang, J.-S., Kuszewski, J., Nilges, M., Pannu, N.S., et al. (1998). Crystallography & NMR system: a new software suite for macromolecular structure determination. Acta Crystallogr. D Biol. Crystallogr. *54*, 905–921.

Burk, D., Hon, W., Leung, A., and Berghuis, A. (2001). Structural analyses of nucleotide binding to an aminoglycoside phosphotransferase. Biochemistry *40*, 8756–8764.

CCP4 (Collaborative Computational Project, Number 4) (1994). The CCP4 suite: programs for protein crystallography. Acta Crystallogr. D Biol. Crystallogr. *50*, 760–763.

Daigle, D.M., McKay, G.A., and Wright, G.D. (1997). Inhibition of aminoglycoside antibiotic resistance enzymes by protein kinase inhibitors. J. Biol. Chem. *272*, 24755–24758.

Enslen, H., and Davis, R.J. (2001). Regulation of MAP kinases by docking domains. Biol. Cell. *93*, 5–14.

Forrer, P., Stumpp, M.T., Binz, H.K., and Plückthun, A. (2003). A novel strategy to design binding molecules harnessing the modular nature of repeat proteins. FEBS Lett. *539*, 2–6.

Forrer, P., Binz, H.K., Stumpp, M.T., and Plückthun, A. (2004). Consensus design of repeat proteins. ChemBioChem *5*, 183–189.

Hon, W., McKay, G., Thompson, P., Sweet, R., Yang, D., Wright, G., and Berghuis, A. (1997). Structure of an enzyme required for aminoglycoside antibiotic resistance reveals homology to eukaryotic protein kinases. Cell *89*, 887–895.

Hubbard, S.R., Wei, L., Ellis, L., and Hendrickson, W.A. (1994). Crystal structure of the tyrosine kinase domain of the human insulin receptor. Nature *372*, 22–29.

Huse, M., and Kuriyan, J. (2002). The conformational plasticity of protein kinases. Cell *109*, 275–282.

Jeffrey, P.D., Tong, L., and Pavletich, N.P. (2000). Structural basis of inhibition of CDK-cyclin complexes by INK4 inhibitors. Genes Dev. *14*, 3115–3125.

Jones, S., and Thornton, J.M. (1996). Principles of protein-protein interactions. Proc. Natl. Acad. Sci. USA *93*, 13–20.

Jones, T.A., Zou, J.Y., Cowan, S.W., and Kjeldgaard, M. (1991). Improved methods for building protein models in electron density maps and the location of errors in these models. Acta Crystallogr. D Biol. Crystallogr. *47*, 110–119.

Kohl, A., Binz, H.K., Forrer, P., Stumpp, M.T., Plückthun, A., and Grütter, M.G. (2003). Designed to be stable: crystal structure of a consensus ankyrin repeat protein. Proc. Natl. Acad. Sci. USA *100*, 1700–1705.

Kuzmic, P. (1996). Program DYNAFIT for the analysis of enzyme kinetic data: application to HIV proteinase. Anal. Biochem. *237*, 260–273.

Lo Conte, L., Chothia, C., and Janin, J. (1999). The atomic structure of protein-protein recognition sites. J. Mol. Biol. *285*, 2177–2198.

Manning, G., Whyte, D.B., Martinez, R., Hunter, T., and Sudarsanam, S. (2002). The protein kinase complement of the human genome. Science *298*, 1912–1934.

McKay, G.A., Thompson, P.R., and Wright, G.D. (1994). Broad spectrum aminoglycoside phosphotransferase type III from *Enterococcus*: overexpression, purification, and substrate specificity. Biochemistry *33*, 6936–6944.

Murshudov, G.N., Lebedev, A., Vagin, A.A., Wilson, K.S., and Dodson, E.J. (1999). Efficient anisotropic refinement of macromolecular structures using FFT. Acta Crystallogr. D Biol. Crystallogr. *55*, 247–255.

Navaza, J. (1994). AMoRe: an automated package for molecular replacement. Acta Crystallogr. A *50*, 157–163.

Navaza, J. (2001). Implementation of molecular replacement in AMoRe. Acta Crystallogr. D Biol. Crystallogr. *57*, 1367–1372.

Noble, M.E.M., Endicott, J.A., and Johnson, L.N. (2004). Protein kinase inhibitors: insights into drug design from structure. Science *303*, 1800–1805.

Otwinowski, Z., and Minor, W. (1997). Processing of X-ray diffraction data collected in oscillation mode. In Methods in Enzymology, C.W. Carter and J. R.M. Sweets, eds. (New York: Academic Press), pp. 307–326.

Ozen, C., and Serpersu, E.H. (2004). Thermodynamics of aminoglycoside binding to aminoglycoside- 3′-phosphotransferase IIIa studied by isothermal titration calorimetry. Biochemistry *43*, 14667–14675.

Pavletich, N.P. (1999). Mechanisms of cyclin-dependent kinase regulation: structures of Cdks, their cyclin activators, and Cip and INK4 inhibitors. J. Mol. Biol. *287*, 821–828.

Pawson, T., and Nash, P. (2003). Assembly of cell regulatory systems through protein interaction domains. Science *300*, 445–452.

Russo, A., Tong, L., Lee, J., Jeffrey, P., and Pavletich, N. (1998). Structural basis for inhibition of the cyclin-dependent kinase Cdk6 by the tumour suppressor $p16^{INK4a}$. Nature *395*, 237–243.

Schindler, T., Bornmann, W., Pellicena, P., Miller, W.T., Clarkson, B., and Kuriyan, J. (2000). Structural mechanism for STI-571 inhibition of abelson tyrosine kinase. Science *289*, 1938–1942.

Sedgwick, S.G., and Smerdon, S.J. (1999). The ankyrin repeat: a diversity of interactions on a common structural framework. Trends Biochem. Sci. *24*, 311–316.

Sharrocks, A.D., Yang, S.-H., and Galanis, A. (2000). Docking domains and substrate-specificity determination for MAP kinases. Trends Biochem. Sci. *25*, 448–453.

Szedlacsek, S.E., Ostafe, V., Serban, M., and Vlad, M.O. (1988). A re-evaluation of the kinetic equations for hyperbolic tight-binding inhibition. Biochem. J. *254*, 311–312.

Tanoue, T., and Nishida, E. (2003). Molecular recognitions in the MAP kinase cascades. Cell. Signal. *15*, 455–462.

Thompson, P.R., Schwartzenhauer, J., Hughes, D.W., Berghuis, A.M., and Wright, G.D. (1999). The COOH terminus of aminoglycoside phosphotransferase (3′)-IIIa is critical for antibiotic recognition and resistance. J. Biol. Chem. *274*, 30697–30706.

Thompson, P.R., Boehr, D.D., Berghuis, A.M., and Wright, G.D. (2002). Mechanism of aminoglycoside antibiotic kinase APH(3′)-IIIa: role of the nucleotide positioning loop. Biochemistry *41*, 7001–7007.

Wang, Z., Harkins, P.C., Ulevitch, R.J., Han, J., Cobb, M.H., and Goldsmith, E.J. (1997). The structure of mitogen-activated protein kinase p38 at 2.1-Å resolution. Proc. Natl. Acad. Sci. USA *94*, 2327–2332.

Accession Numbers

The coordinates and structure factors for the mAPH/AR_3a complex have been deposited in the Protein Data Bank (accession code 2BKK).